



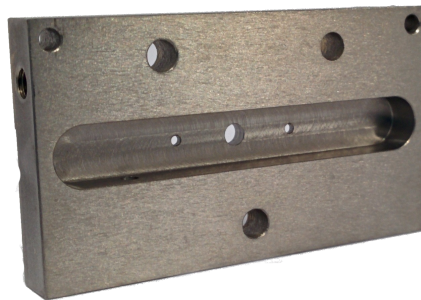
Eidgenössische Technische Hochschule Zürich  
Swiss Federal Institute of Technology Zurich

SEMESTER THESIS

---

# Superconducting 3D Microwave Cavity for QED Experiments with Rydberg Atoms

---



*Author:*  
Andres FORRER

*Supervisor:*  
Mathias STAMMEIER  
Prof. Dr. Andreas WALLRAFF

February 2, 2016

## Abstract

In this semester thesis we investigate the quality factor of a rectangular superconducting 3D microwave niobium cavity used for cavity QED measurements. We show that the resonance frequency of our rectangular cavity in vacuum at 7.2 K is well described by FEM simulations and that we can achieve quality factors of about 1'400'000 in liquid helium for the third mode. Further we measure the losses due to additional copper electrodes placed at the nodes of the third mode which gives a total quality factor of 689'000. Finally we measure the quality factor for the cavity with the copper electrodes and two entrance holes in the cavity for the cavity-Rydberg atom interaction which results in a quality factor of  $Q \approx 608'000$ . This result shows that we should be able to measure in the strong coupling regime and perform dispersive shift experiments with the cavity.

# Contents

<b>1</b>	<b>Introduction</b>	<b>1</b>
1.1	Goal of the <i>Rydberg Project</i> . . . . .	1
1.2	Current state . . . . .	3
1.3	This thesis . . . . .	4
<b>2</b>	<b>Theory</b>	<b>5</b>
2.1	Basics of rectangular 3D cavities . . . . .	5
2.2	Niobium cavity design . . . . .	9
2.3	Cavity electrodes . . . . .	9
2.4	Q factor of superconducting cavities . . . . .	11
2.5	FEM simulations . . . . .	12
<b>3</b>	<b>Measurements</b>	<b>13</b>
3.1	Standard experiment . . . . .	13
3.2	Helium and vacuum measurement . . . . .	15
<b>4</b>	<b>Measurement results</b>	<b>17</b>
4.1	Frequency behavior in vacuum . . . . .	17
4.2	Undercoupled cavity . . . . .	21
4.3	Basic cavity . . . . .	21
4.4	Cavity with electrodes . . . . .	23
4.5	Cavity with Rydberg entrance holes . . . . .	23
4.6	Cavity with electrodes and Rydberg entrance holes . . . . .	25
4.7	Additional measurements . . . . .	26
4.7.1	Power dependence . . . . .	26
4.7.2	Magnetic field . . . . .	27
<b>5</b>	<b>Conclusion and outlook</b>	<b>29</b>
<b>A</b>	<b>Calculation of electrode Q factor</b>	<b>34</b>

# 1 Introduction

In the past decades a lot of research on quantum computing and their practical realization was done in different fields of physics such as trapped ions [1], single spins in semiconductors [2] or photons [3]. Some outlook of quantum information is given by M. H. Devoret [4]. Most of these experiments have their advantages but also their weaknesses and that's why hybrid systems were developed which use the strengths of each type of setup and reduce the negative features [5][6]. The Rydberg Project in the Quantum Device Lab at the ETH Zürich tries to implement a hybrid system consisting of Rydberg atoms and superconducting circuits.

## 1.1 Goal of the *Rydberg Project*

To realize such a hybrid system the Rydberg Project combines the advantages of superconducting qubits with the advantages of Rydberg atoms. Superconducting qubits have the advantage of a strong coupling strength  $g/2\pi \approx 150 \text{ MHz}$  [7] [8], coherence times of up to  $\tau \approx 100\mu\text{s}$  [9], single qubit gate times within 5 to 50 *ns* [4] and a good scalability. Rydberg atoms have a coupling strength of  $g/2\pi \approx 1.5 \text{ MHz}$  [10] and long coherence times up to  $\tau \approx 1 \text{ ms}$ . So the idea is to couple the superconducting qubit via the cavity photons to the Rydberg atoms. This gives the advantages of the stronger coupling strength and the shorter gate time of superconducting qubits and the longer coherence time of Rydberg atoms. The Rydberg atoms are then used to read out the information about the superconducting qubit.

## Jaynes-Cumming-Hamiltonian

The main idea is to couple via a resonator to Rydberg atoms. The Hamiltonian describing a system of  $N$  atoms coupling to  $n$  cavity photons is the Tavis-Cummings-Hamiltonian  $\mathcal{H}_{TC}$  [11][12]. For a single cavity photon ( $n = 1$ ) the Tavis-Cumming-Hamiltonian reduces (approximately) to the Jaynes-Cumming-Hamiltonian

$$\mathcal{H}_{TC} \approx \mathcal{H}_{JC} = \hbar\omega_c a^\dagger a + \hbar\frac{\omega_a}{2}\sigma_z + \hbar g_N (a^\dagger \sigma_- + a \sigma_+) \quad (1)$$

where  $a^\dagger, a$  are the creation and annihilation operator of the cavity field with cavity frequency  $\omega_c$ ,  $\sigma_z$  the Pauli z-operator and  $\sigma_+, \sigma_-$  the creation and annihilation operator of the atom with transition frequency  $\omega_a$ . The first term can be seen as the cavity Hamiltonian, the second part as the atom Hamiltonian and the third as the coupling Hamiltonian. The many atom coupling strength  $g_N$  is given as  $g_N = g_1\sqrt{N}$  with  $g_1 = d_a E_0/\hbar$  the coupling strength of a single atom with dipole moment  $d_a$  coupled to the

rms field  $E_0$  of a single photon inside the cavity.

We further use the uncoupled states  $|e, n \rangle$  and  $|g, n+1 \rangle$  and  $\Delta = \omega_a - \omega_c$  the detuning of the frequencies. Here  $e$  and  $g$  stands for the two level system of the atom and  $n$  and  $n+1$  for the field levels of the cavity. We also define the  $n$ -photon Rabi frequency  $\Omega_n$ :

$$\Omega_n = \Omega_0 \sqrt{n+1} \quad (2)$$

where  $\Omega_0 = 2g_1$  is the vacuum Rabi frequency. We introduce the *mixing angle*  $\Theta_n$  to calculate the eigenenergies and eigenstates of the JC Hamiltonian:

$$\tan \Theta_n = \frac{\Omega_n}{\Delta} \quad (3)$$

If we restrict us to the so called  *$n$ th doublet*, which means fixed photon number  $n$ , the eigenstates and eigenenergies are represented as the following for the Jaynes-Cumming-Hamiltonian [13]:

$$E_n^\pm = (n+1/2)\hbar\omega_c \pm \frac{\hbar}{2}\sqrt{\Delta^2 + \Omega_n^2} \quad (4)$$

and eigenstates:

$$|+, n \rangle = \cos(\Theta_n/2)|e, n \rangle + i\sin(\Theta_n/2)|g, n+1 \rangle \quad (5)$$

$$|-, n \rangle = \sin(\Theta_n/2)|e, n \rangle - i\cos(\Theta_n/2)|g, n+1 \rangle \quad (6)$$

These states are called *dressed states*. An illustration of the eigenstates of the Jaynes-Cumming-Hamiltonian is shown in figure 1. Note that this is true for all  $n$  only if  $N=1$ . For  $N > 1$  and  $n = 0$  we use the approximation  $\mathcal{H}_{TC} \approx \mathcal{H}_{JC}$  where eqn's (4),(5) and (6) would still hold.

For resonant detuning,  $\Delta = 0$ , we observe the splitting of the energy by  $2\hbar g_N$ . For non-resonant detuning,  $\Delta \gg \Omega_n$ , we are in the dispersive limit. Here the dressed states are dominated by the uncoupled states  $|e, n \rangle$  and  $|g, n+1 \rangle$  but have an admixture of the opposite state. Due to this admixture we see a shift in the atomic transition. This can better be seen when we apply the unitary transformation  $U = \exp[\frac{g_N}{\Delta}(a\sigma_+ - a^\dagger\sigma_-)]$  on  $\mathcal{H}_{JC}$  and expand to second order in  $g_N$  [14]:

$$U\mathcal{H}U^\dagger \approx \hbar \left[ \omega_c + \frac{g_N^2}{\Delta}\sigma_z \right] a^\dagger a + \frac{\hbar}{2} \left[ \omega_a + \frac{g_N^2}{\Delta} \right] \sigma_z \quad (7)$$

The shift  $\frac{g_N^2}{\Delta}(n+1/2)$  is interpreted as the ac Stark/Lamb shift of the atom transition. Alternatively we can interpret  $\frac{g_N^2}{\Delta}\sigma_z$  as the dispersive shift of

the resonator transition. By observing the magnitude and the direction of this shift it is possible to read out the dressed states of Rydberg atoms without disturbing them. This shift is best observed in the strong coupling regime where the coupling strength dominates over the present losses and the interaction time, i.e.

$$g_N > \kappa, \gamma_{ns}, \gamma_{np}, T_{int}^{-1} \quad (8)$$

Here  $\kappa$  is the total loss rate of the cavity,  $\gamma_{ns/np}$  the decay time of the ns/np state of the Rydberg atom and  $T_{int}^{-1}$  the inverse interaction time of the Rydberg atoms with the cavity field.

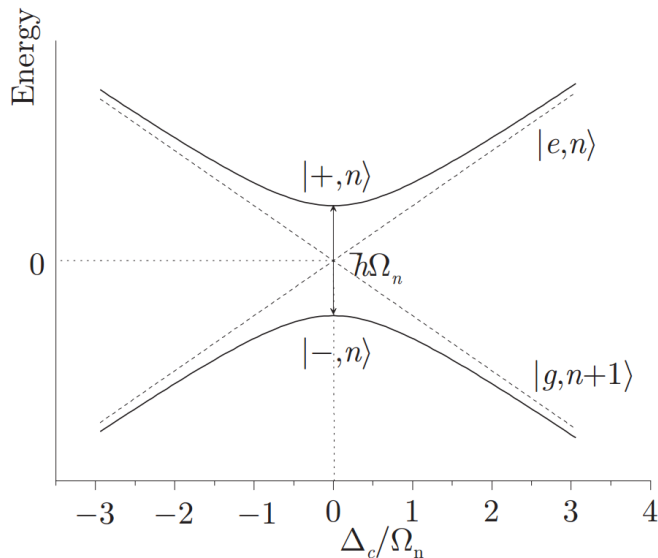


Figure 1: Schematic sketch of the dressed state of the  $n^{th}$  doublet of the Jaynes-Cummings-Hamiltonian. From [13].

## 1.2 Current state

In the Rydberg Project two types of resonators are used. The first is a 2D CPW resonator made of NbTiN where the Rydberg atoms fly above the resonator. The quality factor (Q factor) of this resonator is about 10'000. The resonator has a large microwave field which leads to a strong coupling. The CPW resonator has a typical single atom coupling strength of  $g/2\pi = 1MHz$  at  $20\mu m$  distance above the surface, which exponentially decays with the distance. Close to surfaces the Rydberg atoms experience a DC-shift from electrical stray fields which were studied spectroscopically by Thiele et al. [15].

The second type of resonator is a 3D rectangular copper cavity. The best Q

Table 1: Table of relevant parameters of the experiment.

Name	Parameter	Value
two-level-system	two-level-system	36s-36p
resonator/transition freq.	$\frac{\omega_c}{2\pi} \approx \frac{\omega_a}{2\pi}$	21.530 GHz
dipole moment	$d_a$	1890 $ea_0$
electrical field amplitude	$E_0$	1.25 $\frac{mV}{m}$
JC single coupling strength	$\frac{g^1}{2\pi}$	30 kHz
number of Rydberg atoms	N	1000
coupling strength for many atoms	$\frac{gN}{2\pi}$	1 MHz
inverse interaction time	$T_{int}^{-1}$	0.5 MHz
36s decay rate	$\frac{\gamma_{36s}}{2\pi}$	5 kHz
36p decay rate	$\frac{\gamma_{36p}}{2\pi}$	76 kHz
intern copper cavity loss rate	$\frac{\kappa_{int,Cu}}{2\pi}$	2 MHz
total copper cavity loss rate	$\frac{\kappa_{Cu}}{2\pi}$	4 MHz
intern niobium cavity loss rate	$\frac{\kappa_{int,Nb}}{2\pi}$	35 kHz
total niobium cavity loss rate	$\frac{\kappa_{Nb}}{2\pi}$	70 kHz

factor was about 15'000. The 3D cavity has the advantage of a homogeneous microwave field perpendicular to the beam and typically close to zero stray fields. The Rydberg atom-cavity interaction and the manipulation of the Rydberg atoms through the quadratic AC Stark effect with this copper cavities were mainly examined in the master thesis of S. Ruffieux [16]. Table 1 lists the relevant parameters for the copper cavity. Since  $\kappa_{Cu} > g_N$ , the copper cavities do not fulfill the criterion for the strong coupling regime, eq. (8). That's why a new niobium cavity was designed to perform dispersive shift measurements in the strong coupling regime in the future.

### 1.3 This thesis

In this thesis we examined the Q factor for a superconducting 3D niobium microwave cavity. For that a 3D cavity, based on a previous design of the copper cavities, was constructed. In a first step we measured the temperature dependence of a basic cavity (specified in section 2.3) and compared it to a theoretical model for the Q factor which includes the superconductivity of niobium. In the second step we performed measurements with copper electrodes placed at the nodes of the third cavity mode and compared the results to a theoretical model that explains the change in the Q factor due to losses (see section 2.3). In a third and fourth step we simultaneously measured the Q factor of the cavity with and without the electrodes for different sizes of entrance holes for the Rydberg atoms. In this study we stopped at a certain radius of the entrance hole in order to keep the Q factor above a

threshold of 600'000.

The results showed that the cavity is sufficient to do measurement in the strong coupling regime in terms of the Q factor. This gives the basis to observe the dispersive shift in further measurements.

## 2 Theory

In this section we will present the fundamental equations to determine the resonance frequency and the Q factor of rectangular 3D cavities and will give a model to modify the Q factor equation for superconducting cavities. We will also present a detailed view of the realized niobium cavity. In general we will follow the books of D. Pozar [17] and R. Collin [18].

### 2.1 Basics of rectangular 3D cavities

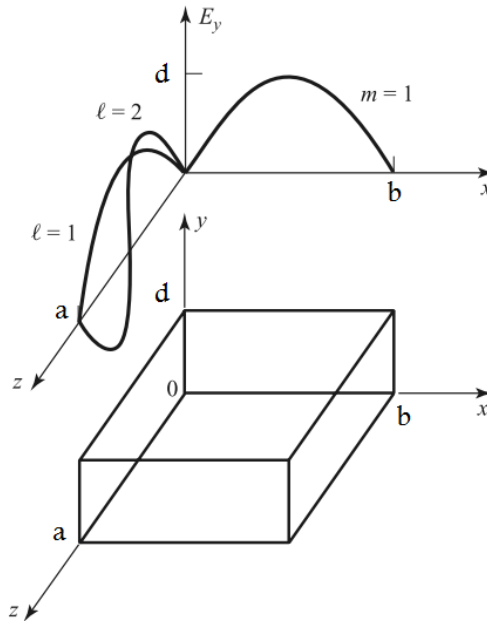


Figure 2: Illustration of a rectangular cavity with edge lengths  $a, b$  and  $d$ . The standing wave in direction of  $a$  ( $l=1$  and  $l=2$ ) and the standing wave in direction of  $b$  ( $m=1$ ) are drawn. From [17] and edited.

For our case we'll concentrate on the analytic solution of a rectangular cavity. We assume a cavity with fixed edge lengths  $a, b$  and  $d$ . In general  $a$  denotes the longest dimension. We derive the following condition for the wave number using the known TE modes for a rectangular waveguide with lengths  $a$  and  $b$  and new boundary conditions for the cavity:



$$k_{mnl} = \sqrt{\left(\frac{m\pi}{a}\right)^2 + \left(\frac{n\pi}{d}\right)^2 + \left(\frac{l\pi}{b}\right)^2} \quad (9)$$

This describes standing waves inside the cavity which are called  $TE_{mnl}$  or  $TM_{mnl}$  modes. Figure 2 illustrates the  $TE_{001}$ ,  $TE_{002}$  and  $TE_{100}$  modes. The indices m,n and l refer to the standing wave pattern in the a,d and b direction. For the resonance frequencies we derive the following equation:

$$f_{mnl} = \frac{c}{2\pi\sqrt{\mu_r\epsilon_r}} \cdot \sqrt{\left(\frac{m\pi}{a}\right)^2 + \left(\frac{n\pi}{b}\right)^2 + \left(\frac{l\pi}{d}\right)^2} \quad (10)$$

where  $\mu_r\epsilon_r$  the relative permeability and permittivity of the dielectrics inside the cavity. For  $TE_{01l}$  modes we can express the electric and magnetic fields analytically:

$$E_y = E_0 \sin \frac{\pi x}{a} \sin \frac{l\pi z}{d} \quad (11)$$

$$H_x = \frac{-iE_0}{Z_{TE}} \sin \frac{\pi x}{a} \cos \frac{l\pi z}{d} \quad (12)$$

$$H_z = \frac{-i\pi E_0}{k\eta a} \cos \frac{\pi x}{a} \sin \frac{l\pi z}{d} \quad (13)$$

where  $\eta = \sqrt{\mu/\epsilon}$  is the intrinsic impedance of the dielectric inside the cavity and  $Z_{TE} = k\eta/\beta$ , where  $\beta = \sqrt{k^2 - (\pi/a)^2}$ . This equation leads to the stored electric/magnetic energy  $W_{e/m}$ :

$$W_e = \frac{\epsilon}{4} \int_V E_y E_y^* dv = \frac{\epsilon abd}{16} E_0^2 \quad (14)$$

$$W_m = \frac{\mu}{4} \int_V (H_x H_x^* + H_z H_z^*) dv = \frac{\mu abd}{16} E_0^2 \left( \frac{1}{Z_{TE}^2} + \frac{\pi^2}{k^2 \eta^2 a^2} \right) \quad (15)$$

By using the definition of  $Z_{TE}$  we find that at resonance  $W_m = W_e$ . The power loss  $P_{loss}$  for the rectangular cavity can be derived for small losses as:

$$P_{loss} = \frac{R_S}{2} \int_{Walls} |H_t|^2 ds \quad (16)$$

with  $R_S = \sqrt{\omega\mu_0/2\sigma}$  the surface conductivity and  $H_t$  the magnetic field tangential to the surface.

So far we can use the definition of the quality factor Q:

$$Q = \omega \frac{\text{average stored energy}}{\text{energy losses/second}} = \omega \frac{W_m + W_e}{P_{loss}} \quad (17)$$

where  $W_{m/e}$  is the magnetic/electric energy stored in the cavity and  $P_{loss}$  the energy loss per second. At resonance we use  $W_m = W_e$ .

The Q factor can also be expressed as a loss rate:  $\frac{\kappa}{2\pi} = \frac{\nu_c}{Q}$ . Since loss rates are additive we are able to split the loss rate in external and internal loss rates  $\kappa = \kappa_{int} + \kappa_{ext}$ . This leads to the definition of the internal and external Q factor  $Q_{int}$  and  $Q_{ext}$  with the relation  $\frac{\kappa_{int}}{2\pi} = \frac{\nu_c}{Q_{int}}$  and  $\frac{\kappa_{ext}}{2\pi} = \frac{\nu_c}{Q_{ext}}$ . Since the internal and external loss rates are additive we find the reciprocal relation of the total Q factor with the internal and external Q factors:

$$\frac{1}{Q} = \frac{1}{Q_{int}} + \frac{1}{Q_{ext}} \quad (18)$$

Further on we define the coupling coefficient G:

$$G = \frac{Q_{int}}{Q_{ext}} \quad (19)$$

By using the coupling coefficient we can define three regimes for a resonator:

- overcoupled:  $G \gg 1 \Rightarrow Q \approx Q_{ext}$
- critically coupled:  $G \approx 1 \Rightarrow Q_{int} \approx Q_{ext}$
- undercoupled:  $G \ll 1 \Rightarrow Q \approx Q_{int}$

Using eq. (16), (11), (12) and (13) we get the analytic solution of the Q factor for the  $TE_{01l}$  modes of a rectangular cavity:

$$Q_{int} = \frac{\eta}{2\pi^2 R_S} \cdot \frac{(k_{10l} ad)^3 b}{2l^2 a^3 b + 2bd^3 + l^2 a^3 d + ad^3} \quad (20)$$

The lengths a,b and d are fixed parameters for a given cavity (good assumption for negligible thermal expansion) and the parameter  $\eta$  and the indices m,n,l do not change for examination of one specific cavity resonance. If this assumption holds the quality factor in eq. (20) only depends on the surface resistance  $R_S = \sqrt{\omega\mu_0/2\sigma}$  where  $\sigma$  is the conductivity of the cavity material. We note that this formula is for non-superconducting materials. A model to describe the surface resistance of superconducting materials is presented in section 2.4. We conclude the following statement: A smaller surface resistance leads to a higher quality factor for fixed side conditions. Further on the Q can be written as:

$$Q = \frac{\nu_r}{\Delta\nu_r} \quad (21)$$

where  $\nu_r$  is the resonance frequency and  $\Delta\nu_r$  is the half-power fractional bandwidth (see figure 3). This gives a simple method to measure the Q factor of the cavity by analyzing its frequency spectrum. The frequency spectrum can readily be measured by a vector network analyzer (VNA). The data obtained from the VNA is fitted to a Lorentzian shape of the resonance to determine  $\nu_r$  and  $\Delta\nu_r$ :

$$F_L = \frac{|S_{21}(\nu_r)|^2}{\left(\frac{\nu-\nu_r}{\Delta\nu_r/2}\right)^2 + 1} \quad (22)$$

where  $S_{21}(\nu_r) =: T(\nu_r)$  is the transmission coefficient at resonance frequency. For such measurements we can write the coupling coefficient G, according to [17], as:

$$G = \frac{\sqrt{T(\nu_r)}}{1 - \sqrt{T(\nu_r)}} \quad (23)$$

Combining (18),(19) and (23) we obtain:

$$Q_{int} = \frac{Q}{1 - T(\nu_r)} \quad (24)$$

$$Q_{ext} = \frac{Q}{T(\nu_r)} \quad (25)$$

We conclude that for direct  $Q_{int}$  measurement we want the system to be undercoupled. Further on we define the insertion loss IL:

$$IL = -10\log(T(\nu_r))dB \quad (26)$$

Additional losses can be caused by dielectric materials inside a cavity. In our measurements we deal with a vacuum or helium filled cavity. This leads to an additional term  $1/Q_{helium}$  in (18).  $Q_{helium}$  is given by the loss tangent of helium [19]:  $\tan(\delta) \simeq 10^{-10} \rightarrow Q_{helium} = \frac{1}{\tan(\delta)} \simeq 10^{10}$ . We can neglect this term in our measurement since we are in the range of  $Q = 10^6$  for this cavity. In the main experiment the cavity will be in vacuum, so this loss due to the helium will disappear.

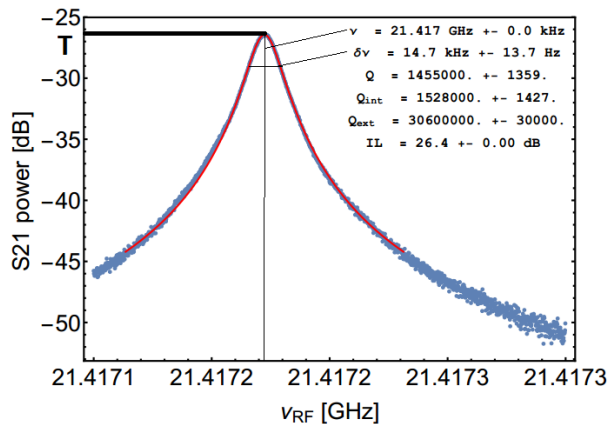


Figure 3: Measured Q factor of mode 3 of the niobium cavity at 4.2 K in helium. The Q factor is determined by equation (21).  $\Delta\nu_r$  ( $\delta\nu$ ) and  $\nu_r$  ( $\nu$ ) are illustrated.

## 2.2 Niobium cavity design

For this experiment a cavity, based on the theoretical considerations in [16], is constructed. The 3D design can be seen in figure 4. The dimensions of the cavity are  $a=43\text{mm}$ ,  $b=6\text{mm}$  and  $d=8\text{mm}$ . The cavity is produced out of a bulk of niobium with purity 99.99 %. Niobium is a superconductor of type II with critical temperature  $T_c = 9.25\text{K}$  [20] and is expected to give a much higher quality factor for the cavity.

## 2.3 Cavity electrodes

Further on we insert two electrodes into the cavity. The placement of the electrodes is at the nodes of mode 3 as shown in figure 6. These electrodes will be needed in the main experiment of the Rydberg Project in order to change the energy states of the Rydberg atoms according to the quadratic AC Stark effect by applying an electrical field. The electrodes will be connected to a SRS SIM928 voltage source with 1 mV resolution. The electrodes are made of copper and have a length of 8.00 mm and a diameter 0.5 mm. With the placement and the small diameter of the electrodes they have a much smaller effect on the mode function of mode 3 than for the other  $TE_{10l}$  modes.

The electrodes lead to an additional loss rate in the cavity. This is associated to an electrode Q factor  $Q_{ele,theo.}$  of the cavity, i.e.  $1/Q = 1/Q_{int} + 1/Q_{ext} + 1/Q_{ele,theo.}$ . Integrating eq. (16) for the electrodes and the third mode, taking into account the temperature dependent conductivity of copper, leads

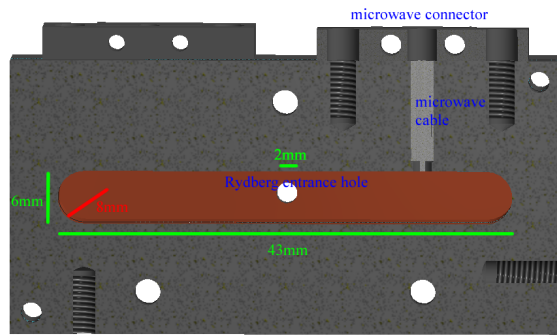


Figure 4: Model of the cavity.

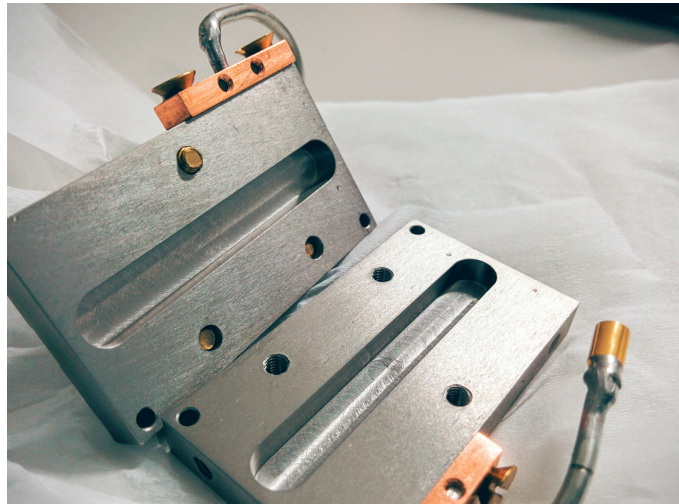


Figure 5: Picture of the niobium cavity used in the experiment without entrance holes for the Rydberg atoms.

to the following result for the pure electrode Q factor:

$$Q_{ele,theo.} = 1.497 * 10^6 \quad (27)$$

for  $\sigma_{Cu} = 2.33 * 10^8 S/m$  for copper at 4.2 K obtained from previous Q factor measurements of copper cavities. The detailed calculation is in the appendix A. Here we assume that the electrodes do not significantly change the mode function inside the cavity. This is justified for mode 3 as the HFSS simulation in figure 6 shows.

Further on we will refer the niobium cavity without any electrode and without any additional holes as the basic cavity. Figure 5 shows the basic cavity. By comparing the Q factor of mode 3 for the basic cavity in the HFSS simulation with the Q factor from the simulation of the cavity with the electrodes, using  $\sigma_{copper} = 2.33 * 10^8 S/m$  and eq. (18), we find the associated electrode Q factor:

$$Q_{ele,sim.} = 1.379 * 10^6 \quad (28)$$

Since  $\sigma_{Cu}$  will not significantly change for lower T this is an universal value for the electrode Q factor and for that a fixed loss. Because  $\sigma_{Nb}$  does significantly depend on the temperature it is good to know this temperature independent electrode Q factor.

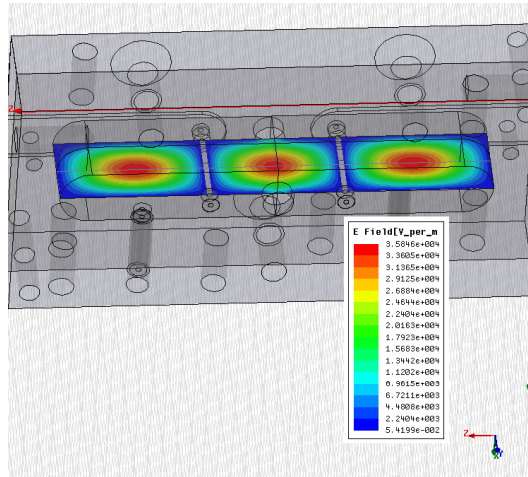


Figure 6: Model of the cavity.

## 2.4 Q factor of superconducting cavities

For superconducting niobium the surface resistance  $R_S$  in eq. (20) has to be replaced by an effective model from the literature: [21].

$$R_S = R_{BCS} + R_0 = \frac{A}{T} \nu^2 \exp[-\Delta(T_c)/k_B T] + R_0 \quad (29)$$

where  $A$  is a material constant,  $T$  the temperature,  $k$  the Boltzmann constant,  $\Delta(T_c) = B \cdot k_B T_c$  the  $T_c$ -dependent energy gap of niobium with  $B$  a material dependent constant and  $R_0$  the residual resistance. The model is valid for  $\nu \ll 2\Delta/h \approx 10^{12} Hz$  and  $T_c/T > 2$ . This model is based on cooper pairs which are used to describe superconducting materials [22]. A qualitative understanding of eq. (29) is the following[22]:

At  $T=0$  K all electrons have formed cooper pairs, which form a superfluid, due to their bosonic nature, with zero resistance. For increasing  $T$  the fraction of unpaired electrons increases with  $e^{-\Delta/kT}$ .  $2\Delta$  is the energy gap of the superconductor or in other words the energy needed to break up one cooper pair. In a dc field the cooper pairs carry all the current and because cooper pairs move without friction there is no resistance. If a RF field is applied the cooper pairs are constantly changing their direction and due to the internal mass of the cooper pairs a force must be applied to bring an alternating direction of current flow. For that an AC field will be present and accelerates the normal electrons leading to a finite resistance. This resistance is proportional to the square of the RF frequency  $\nu$ . Above  $T_c$  there are no cooper pairs and we are back in the normal conducting regime of the material.

The residual resistance  $R_0$  depends on many material parameters but mainly on impurities. These impurities give a limitation of the minimal achievable surface resistance for  $T \rightarrow 0$ . Basically we can say that a higher RRR value (**r**esidual **r**esistance **r**atio, indicating the purity of a material) leads to a smaller residual resistance.

The superconductivity leads to very high Q factors of cavities. Q factors up to  $10^{11}$  were measured in accelerator physics [23],[24],[25].

## 2.5 FEM simulations

The first four  $TE_{10l}$  modes of the 3D Cavity are simulated with Ansys HFSS using a discrete sweep with linear steps. Table 2 gives the parameters used in the simulation. Figure 7 shows the electrical field of mode 3. The simulation gives the following resonance frequencies for each mode:

$$\nu_{c1,sim} = 18.853 \text{ GHz} \quad (30)$$

$$\nu_{c2,sim} = 19.857 \text{ GHz} \quad (31)$$

$$\nu_{c3,sim} = 21.430 \text{ GHz} \quad (32)$$

$$\nu_{c4,sim} = 23.454 \text{ GHz} \quad (33)$$

The resonance frequencies calculated from theory, using eq. (10), are the

following ones:

$$\nu_{c1,theo} = 19.072 \text{ GHz} \quad (34)$$

$$\nu_{c2,theo} = 20.006 \text{ GHz} \quad (35)$$

$$\nu_{c3,theo} = 21.473 \text{ GHz} \quad (36)$$

$$\nu_{c4,theo} = 23.372 \text{ GHz} \quad (37)$$

Table 2: Relevant parameter used in the HFSS simulation.

	Relative Permittivity	Relative Permeability	Bulk Conductivity	Dielectric Loss Tangent
Copper 300 K	1	0.999991	$5.8 \cdot 10^7$ s/m	0
Copper 4K	1	0.999991	$23.2 \cdot 10^7$ s/m	0
Niobium	1	1	$1.9 \cdot 10^{12}$ s/m	0
Teflon	2.1	1	0	0.001
Vacuum	1	1	0	0
Peek	3.5	1	0	0.004

### 3 Measurements

#### 3.1 Standard experiment

The measurements are done in a helium dewar with a dipstick. The niobium cavity is connected via a copper piece to the dipstick. A temperature sensor is connected at the bottom of the cavity. Two stainless steel microwave cables are installed inside the dipstick for S-parameter measurements. Additionally there are four copper DC wires for optional measurement extensions. The schematic setup is sketched in figure 8.

The coupling cable pins are slightly placed inside the cavity to achieve an undercoupled cavity. The two (optional) amplifiers (amplifier 1 & 2) lead to an increased  $S_{21}$  of about 28 dB each in the frequency range from 18 to 25 GHz. The used settings are mentioned at the end of this section. **Important:** the supply box Bias Box LNF S0012 has not the same positions as Bias Box LNF S0010 and can cause a damage of the amplifiers! The amplifier enhances the signal-to-noise ratio in the transmission parameter  $S_{21}$ . This follows from noise temperature [17]:  $T_{noise} = \frac{N_0}{Gk_B BW}$  with BW the band width, G the gain and  $N_0$  the noise power. The over all noise temperature is typically dominated by the first amplifier noise temperature. In a first step we fully insert the cavity into helium to efficiently reach a cavity temperature of 4.2 K. In a second step we slowly pull out the cavity until we see an increase in temperature. At this point we slightly pull back the cavity such that the temperature sensor and the bottom of the cavity are



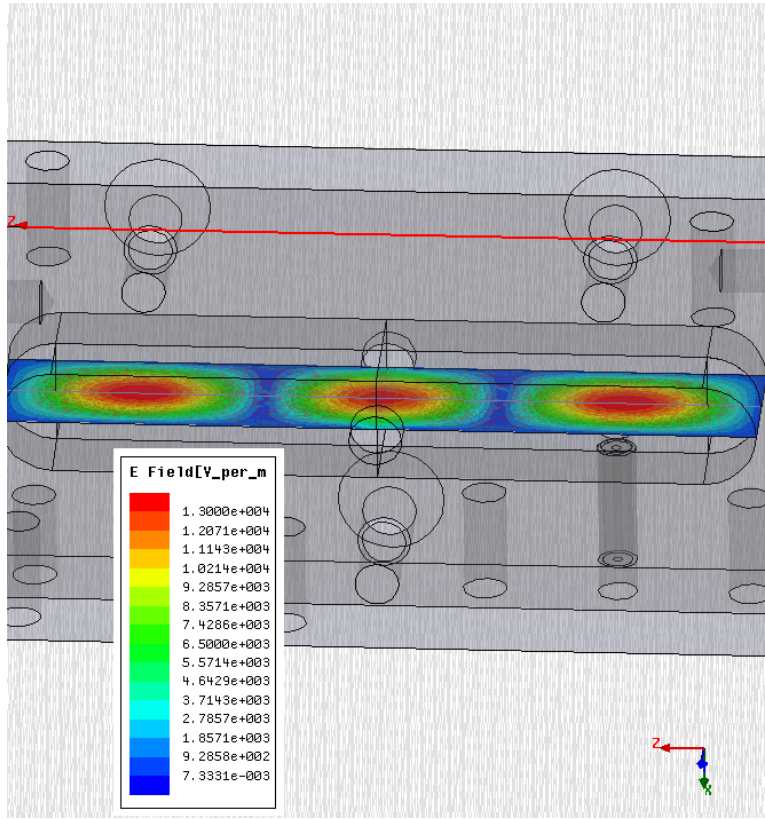


Figure 7: Simulated electrical fields for mode 3.

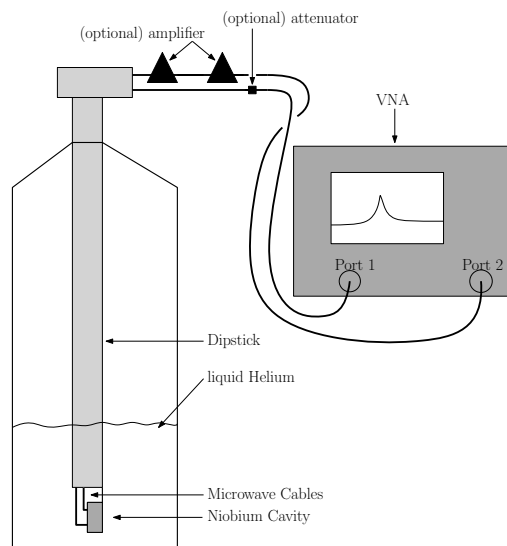


Figure 8: Setup of the dipstick measurement.

in helium. This leads to a direct cooling of the cavity without having liquid helium inside. We will refer this as the standard measurement in helium (SMH) situation. One may ask why we do not want to have liquid helium inside the cavity. The reason is that we observe a jiggling and oscillation of the resonance frequency if the cavity is completely inside the liquid helium. In this case we are not able to perform an accurate measurement. This may be caused by the leaky cavity and slowly entering helium. We also observe an increase of this jiggling for small vibrations. Further on we perform a two port measurement with a vector network analyzer (VNA) at a constant temperature. The VNA is controlled via a LabView Software and stores the data into a txt-file containing the frequency and the corresponding transmission or reflection coefficient. In our case we are interested in the  $S_{21}$  transmission coefficient.

The stored data is further analyzed with a Mathematica file. Here we subtract or add the transmission coefficient of the previously measured additional components in the two port circuit, i.e. coupling cable, dipstick cable, amplifiers etc. Then the data is fitted according to eq. (22) from where we obtain the Q factor of the cavity.

**Used Components:**

Amplifier 1 & 2	model <i>TGA4507</i> connected to power supply <i>Bias Box LNF S0010</i> with D=6/10 (3V) and G=5/81 (-130mV) where D: the Drain position and G: the gate position.
Temperature Sensor	maximal output power threshold = 12 dBm DT-670C-Cu from Lake Shore Cryotronics connected to Lake Shore model 325 curve 02 DT-670 off-set 0.19 K from comparison of theoretical [26] and measured liquid helium temperature.
HEMT	connected to power supply <i>Bias Box LNF S0012</i> with D=6/10 (1.2 V) G=6/80 (1.6 V)

### 3.2 Helium and vacuum measurement

For the following we will denote measurements with the complete cavity inside the liquid helium with LHE and in helium vapor with HEV. We can put a brass cylinder over the cavity and evacuate the whole system. The advantages are a stable resonance frequency and a better control and reliability of the temperature sensor. Compare also figure 9. The disadvantages are a longer preparation and cooling time, a higher equilibrium tempera-

ture and less space for all components compared to the SMH. The lowest achieved temperature in vacuum is 5.1 K which corresponds to a Q factor of 1'083'000, where in SMH the highest achieved Q factor was about 1'963'000 for 4.2 K.

The advantages of the SMH are a better cooling, more space, a good adjustment of the temperature from 9.25 K to 4.2 K and a time efficient preparation and measurement. The disadvantages are that helium or helium vapor enters the cavity and that the uncertainty of the temperature measurement is higher. The influence of liquid helium inside the cavity is discussed in section 4.1.

Because of the time efficiency and the higher achievable Q factors we decided to do most of the experiments with the SMH method described in section 3.1 and accepted the consequence of a lower confidence in the temperature. If high accuracy in temperature or frequency was needed we performed the measurement in vacuum.

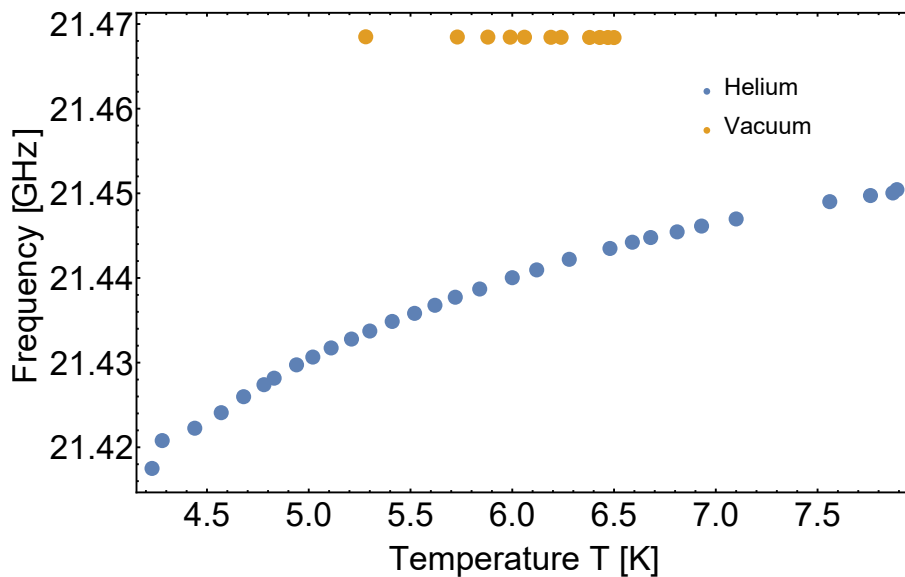


Figure 9: The figure shows the resonance frequencies of mode 3 for the measurement in helium vapor and in vacuum for decreasing temperature. The frequency in helium is decreasing over multiple MHz during the measurement. In contrast the resonance frequency in vacuum stays basically constant.

## 4 Measurement results

### 4.1 Frequency behavior in vacuum

Since the cavity will be in vacuum in the main experiment with a lower temperature we analyze the temperature behavior of the frequency and at a fixed temperature more closely. First we compare the resonance frequency of each mode with the analytic formula, eq. (20), and the simulation. The result from the vacuum measurement at 7.2 K and the simulated and theoretical values for the resonance frequencies are summarized in table 3. Figure 10a shows the difference from the measured resonance frequency at 7 K to the analytic formula and the simulation at 300 K and the modified values at 7 K in figure 10b.

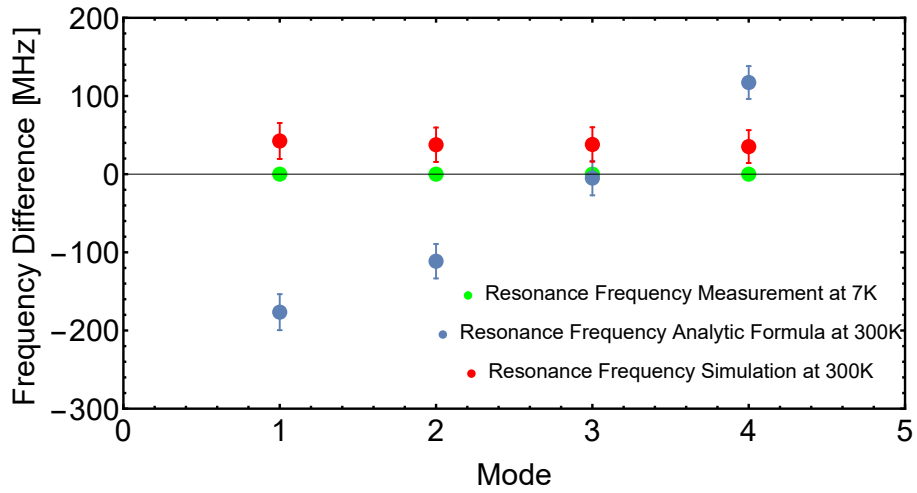
Table 3: Comparison of analytic formula and simulated resonance frequency to the measurement at 7.2 K in vacuum.

	mode 1 [GHz]	mode 2 [GHz]	mode 3 [GHz]	mode 4 [GHz]
formu.	19.072	20.006	21.473	23.372
sim.	18.853	19.857	21.430	23.454
meas.	18.89546 $\pm 0.10 \text{ kHz}$	19.89463 $\pm 0.02 \text{ kHz}$	21.46798 $\pm 0.03 \text{ kHz}$	23.48925 $\pm 0.08 \text{ kHz}$

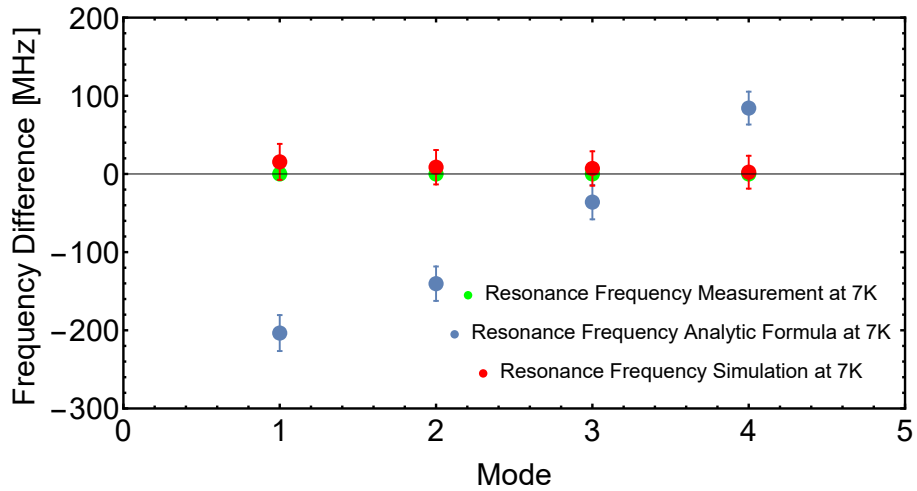
We see that the difference of the simulation for all modes at 300 K is about 40 MHz in the same direction. Therefore we suppose that the differences come from the thermal expansion of the niobium which is not considered in the simulation. And indeed we find a frequency change of 27 to 33 MHz for the different modes by considering linear thermal expansion of niobium using the formulas (38) and (39) below. Further on we have a fabrication tolerance of one-hundredth of a millimeter. This leads to an additional uncertainty of 21 to 23 MHz for the four modes. With the correction of the frequency due to thermal expansion and the uncertainty due to fabrication tolerances we find an agreement of the resonance frequency from the simulation and the measurement as can be seen in figure 10b.

For completeness figure 11 shows the difference from the resonance frequency in vacuum and the resonance frequency in liquid helium with (red) and without (blue) the modification of eq. (10) with  $\epsilon_r = 1.0492$  of liquid helium [27]. We see that the relative permittivity explains the observed change in frequency for the LHE measurements.

Secondly we look at the frequency change in vacuum for decreasing temperature. As figure 12 shows there is a frequency shift in a range smaller than 100 kHz from 6.5 K down to 5.28 K. We find for the slope  $\beta = -73.63 \text{ kHz K}^{-1}$  for a linear fit of the data. This value is interesting in the main experiment to estimate the resonance frequency fluctuations due to thermal fluctuations.



(a) Difference from measured resonance frequency at 7 K and the analytic formula and the simulation at 300 K.



(b) Difference from measured resonance frequency at 7 K and the analytic formula and the simulation modified with a linear thermal expansion of the cavity from 300 K to 7 K.

Figure 10: Difference of measured resonance frequency and the analytic formula and simulation.

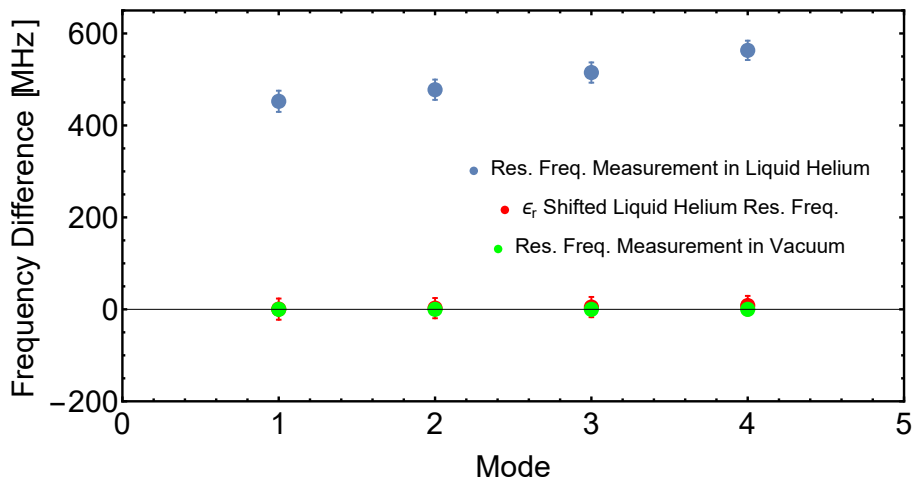


Figure 11: Difference from the measured resonance frequency in vacuum and the measured resonance frequency in liquid helium. The red circles include the shift due to the relative permittivity of liquid helium.

Assuming thermal fluctuations of 100 mK, as estimated for the copper measurement, we would find frequency fluctuations of 7.36 kHz. The frequency change is explained due to the thermal expansion of the niobium. We use the model of linear expansion and an empiric value for the change in length from 300 K to 4 K [37]:

$$\alpha = \frac{1}{L} \frac{\partial L}{\partial T} \approx \frac{1}{L} \frac{\Delta L}{\Delta T} \quad (38)$$

$$\Delta L / L_{300\text{ K}} = 1.43 \cdot 10^{-3} \quad (39)$$

where  $L$  is the initial length and  $\alpha$  the linear expansion coefficient for niobium in each direction. Fitting the model to our data we obtain for the expansion coefficient  $\alpha = 3.4247 \cdot 10^{-6} K^{-1}$ . If we compare to a literature value [28],  $\alpha = (0.01 - 0.003) \cdot 10^{-6} K^{-1}$ , we see a clear difference. The measured value correspond more to the measured expansion coefficient at 70 K from [29]. It has to be mentioned that there are quite different values for different measurements [30] [28] [31] or [29] but, compared to all, our measured expansion coefficient is too large.

When we now look at a fixed temperature  $T$  we would expect to see no change of frequency. And that is exactly what we see in figure 13. The Frequency for one mode stays constant within the error for a fixed temperature.

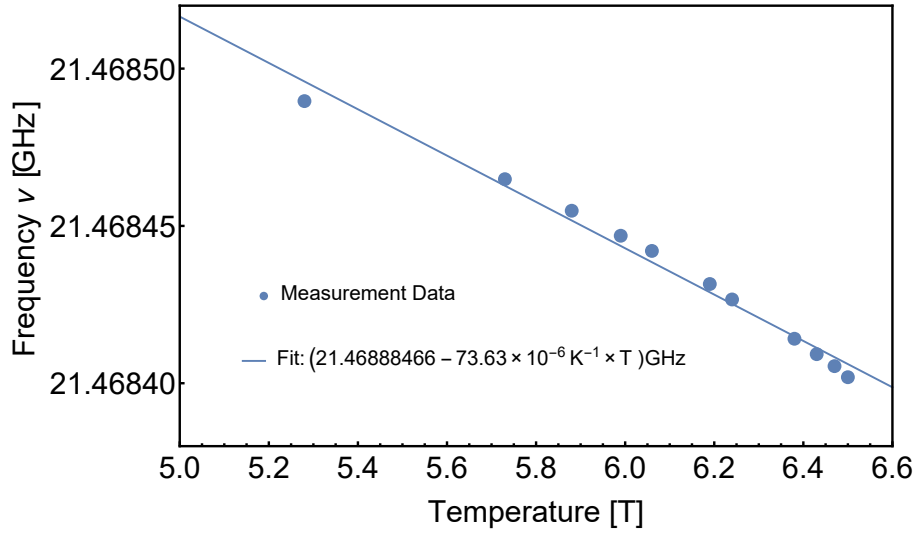


Figure 12: Measured frequency shift on temperature and linear fit. The slope of the fit is  $-73.63 \text{ kHz K}^{-1}$

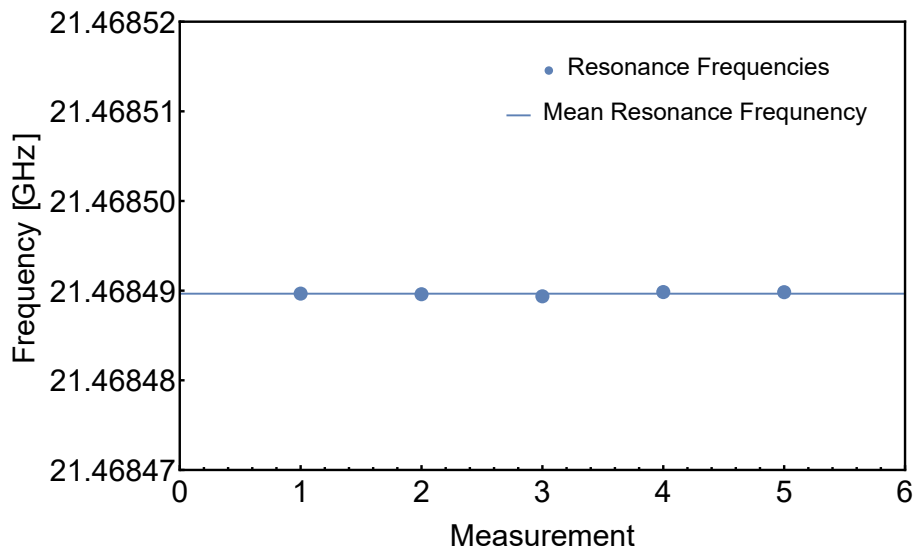


Figure 13: The figure shows the resonance frequencies of mode three for multiple measurements at a fixed temperature  $t=5.28 \text{ K}$ . As expected the frequency is constant up to 1 kHz.

## 4.2 Undercoupled cavity

To directly measure the internal Q factor we undercouple the cavity. Figure 14 shows the internal, external and total Q factor in a log plot. We see that the external Q factor stays constant whereas the internal and total Q factor are close to each others and show the same behavior for decreasing temperature. This indicates that we measure in the undercoupled regime.

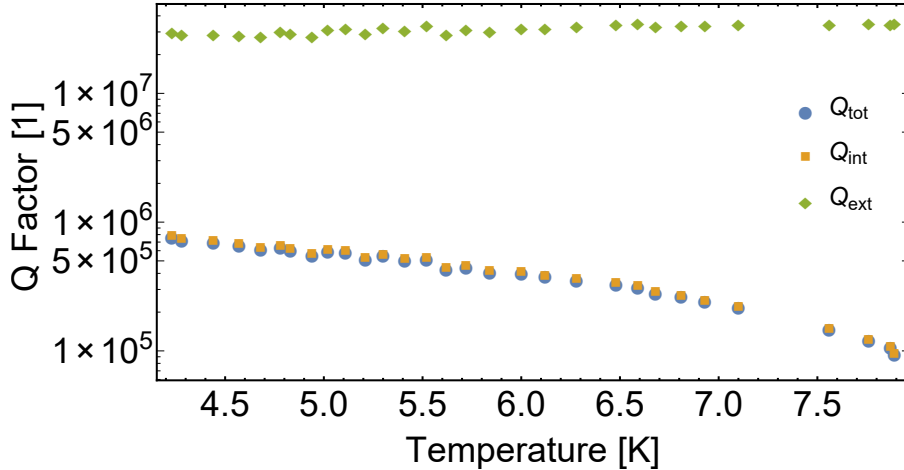


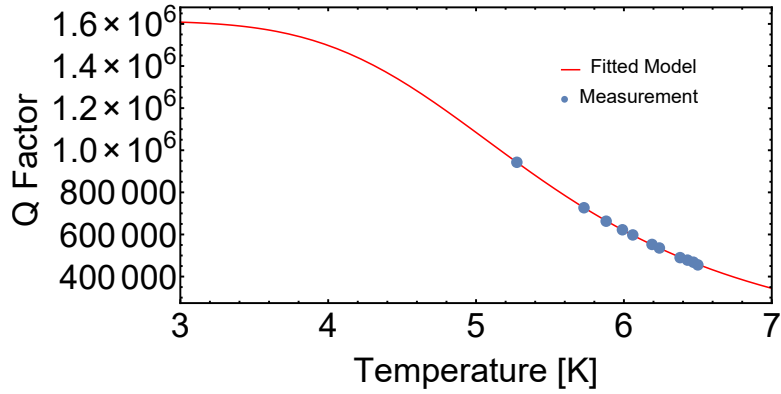
Figure 14: Plot of the total, internal and external Q factor for changing temperature with electrodes.

## 4.3 Basic cavity

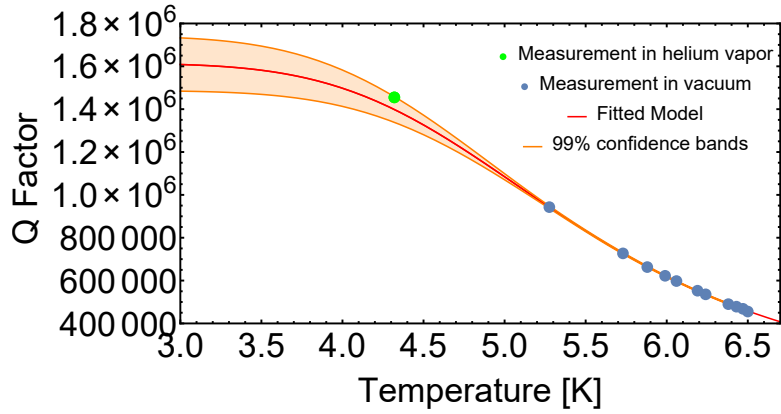
### Temperature dependent Q factor measurement

Further on we want to describe the temperature dependence of the Q factor for the superconducting cavity. For that we measure the Q factor of the cavity in vacuum for different temperatures and fit the obtained data the analytic equation for the Q factor, eq. (20), including the model for the superconducting surface resistance, eq. (29). The fit parameters are  $R_0$ ,  $\Delta$ ,  $A$  and  $T$ . Figure 15a shows the fitted model of the data. Figure 15b shows an additional Q factor of a helium measurement which is not included in the fit. We see that the measurement can not exactly predict the Q factor for lower T. An explanation is that we do not reach sufficient low temperatures in the dipstick measurement in vacuum to fulfill the condition for the surface resistance model ( $T_c/T > 2$ ). This could lead to the difference of the prediction and the helium measurement. For further analysis the measurement has to be repeated in the main experiment of the Rydberg Project where we fulfill the condition for the model.





(a) Fitted Q factor model to the measured data in vacuum.  $A = 3.54 \cdot 10^{-3} Hz^2 K^{-1}$ ,  $\Delta(T_c) = 4.46 k_B T_c$  and  $R_0 = 1.78 * 10^{-4} \Omega$



(b) Fitted Q factor model to the measured data in vacuum. Data point at 4.32 K is in helium and is not included in the fit. The confidence band indicates that there is a larger error at lower temperature.

Figure 15: Fitted Q factor model for superconducting surface resistant.

#### 4.4 Cavity with electrodes

In the previous measurement with the basic cavity we observed a maximal Q factor of 1'474'000. In the next step we prepare the cavity with two copper electrodes at the nodes of the third mode. We then measure the Q factor for this new system and apply different voltages at the electrodes. The results are presented in figure 16 and do not show as significant change for the cavity with the electrodes by changing voltages. Taking the average over all Q factors of the cavity with electrodes gives a mean total Q factor  $Q_{tot,ele} = 689'000 \pm 32'000$

As described in section 2.3 we can identify the loss due to the electrodes with an external Q factor  $Q_{ele,meas.}$ . Using equation (18) we obtain:

$$Q_{ele,meas.} = 1'293'000 \pm 113'000 \quad (40)$$

The comparison of the measured Q factor with the analytic formula, (27), and the simulation in HFSS, (28), shows a reasonable and quantitative agreement:

$$Q_{ele,theo.} = 1'497'000 \quad (41)$$

$$Q_{ele,sim.} = 1'379'000 \quad (42)$$

With this result we have our upper bound in the Q factor due to the losses of the electrodes.

#### 4.5 Cavity with Rydberg entrance holes

In this section we discuss the dependence of Q factor on Rydberg atom entrance holes. The main goal is to have an entrance hole as large as possible while still having a high Q factor to measure in the strong coupling regime. Therefore we simulate the cavity for different entrance hole diameter in HFSS. The evolution of the Q factor is illustrated in figure 17. The simulation shows that the Q factor starts to decrease for an entrance hole diameter larger than 2.0 mm. The conductivity in this simulation is chosen to result in a higher Q factor than in the measurement. Because of this higher Q factor the effect of the entrance hole is observed more clearly than in the measurement but it also makes a direct comparison more complicated. An estimate of the correctness of the simulation gives the microwave wavelength  $\lambda$ . The wavelength is about  $\lambda = 14 \text{ mm}$  and if the diameter gets larger than  $\lambda$  we expect an out coupling through the entrance holes.

The measurement started with an entrance hole width of 0.50 mm which then is successively increased by simultaneously measuring the cavity Q factor with and without the electrodes. The measurement with the electrodes

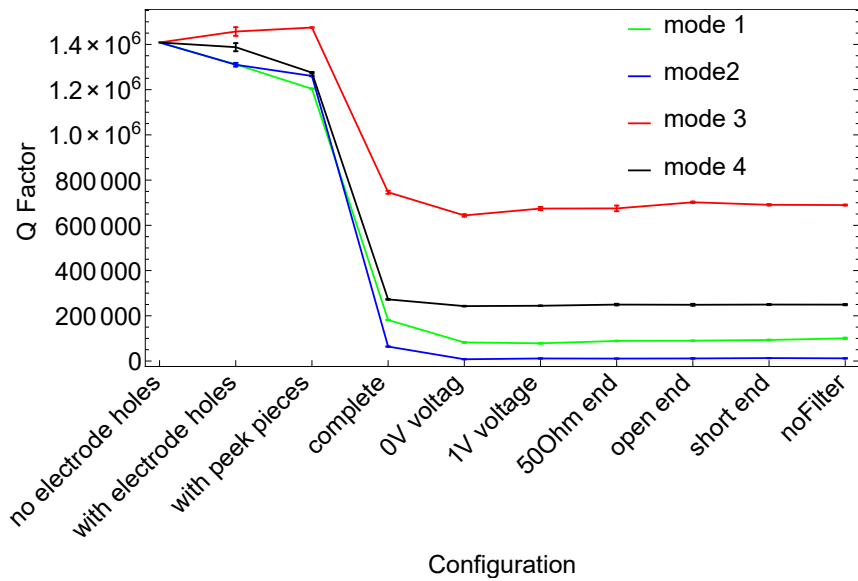


Figure 16: Overview of the Q factors for different cavity configurations. If the electrodes are not inserted in the cavity we get a Q factor of about 1'474'000. The holes for the electrodes and also the peak pieces give a slight change in the Q factor. The third mode is even increasing. After inserting the two electrodes we see the expected decrease of the Q factor.

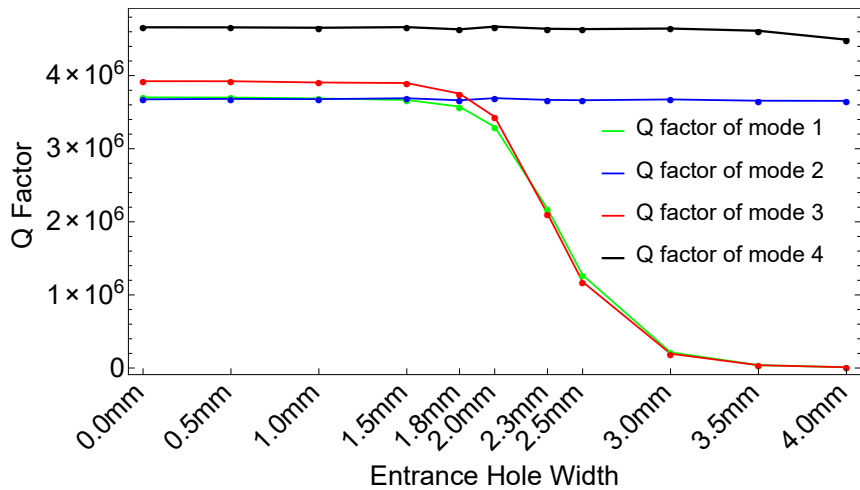


Figure 17: Simulated Q factors for different entrance hole width without electrodes. In the region from 0.0mm to 1.8mm we observe no significant change due to the entrance holes. From 1.8mm to 4.0mm the Q factor for mode 1 and 3 decreases nearly to 0. Mode 2 and 4 are basically unchanged for the simulated diameters.

is analyzed in the next section. The Q factors show the predicted behavior from the simulation up to 1.8 mm. After the 1.8 mm measurement we observed a fraying of the screw thread and fixed them. This fraying was caused by too short screws of length 6 mm which were used in the vacuum measurement to stick copper plates on both sides of the cavity. With the fixed cavity and longer screws of length 8 mm we can increase the clamping pressure of the two cavity halves. For the measurement for a diameter of 2.00 mm we observed an increase of the Q factor in all modes. Since the increase occurred in all modes we assume that it was mainly caused by the higher clamping pressure and not by the entrance holes. At a diameter of 2.30 mm we observed a decrease in the Q factor in mode 1 and 3 whereas mode 2 and 4 stayed constant within the error. Because we only observed the decrease in mode 1 and 3 we assume that this was now a consequence of the entrance holes. Since we want a higher Q factor for the main measurement we stopped the increasing of the holes at this point. The diameter is large enough for the Rydberg atoms to travel through with a negligible stray field.

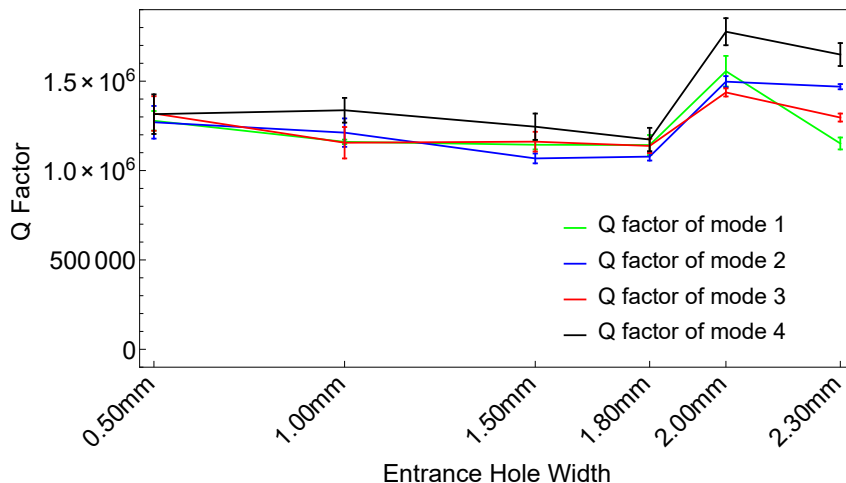


Figure 18: Measured Q factors for different entrance hole widths without electrodes. At the entrance hole width of 1.80mm we observed a fraying of the screw thread. The screw threads were fixed and longer screws were used. At 2.00 mm we observe an increase in all four modes and at 2.30 mm a decrease in mode 1 and 3 and constant behavior for mode 2 and 4.

#### 4.6 Cavity with electrodes and Rydberg entrance holes

As mentioned before we also measured the Q factor for the cavity with the electrodes. In the regime from 0.50 mm up to 1.80 mm we saw the constant behavior of the Q factor as expected from the simulation. At 2.00 mm we

saw again an increase of the Q factor as discussed in the previous section. At 2.30 mm we observed a slight decrease of the Q factor of mode 1 and 3. Surprisingly there was a relative large increase of the Q factor of mode 2 at 2.30 mm diameter entrance holes. Since we did not observe a special change of the Q factor in the measurement without electrodes, see figure 18, we assume that the geometry of the cavity gives such a change of the mode function that the loss through the electrodes decreases and overcompensate any loss through the entrance holes. Because we are mainly interested in mode 3 in the main experiment we did not further investigate this special behavior of mode 2. From this measurement we obtain our final Q factor which is sufficient for the measurements in the main experiment:

$$Q = 608'000 \pm 12'000 \quad (43)$$

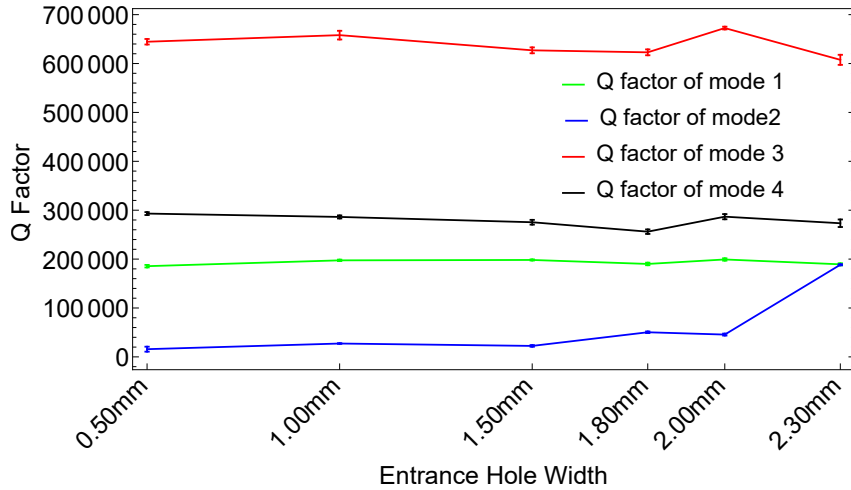


Figure 19: Measured Q factors for different entrance hole widths with electrodes.

## 4.7 Additional measurements

### 4.7.1 Power dependence

To have a high signal-to-noise ratio and for that a good resolution of the Q factor we perform the standard measurement with an input power of -10 dBm. To make sure that we do not have any energy dependent Q factor, meaning a dependence on the photon number inside the cavity, we do a measurement on mode 3 for different input powers. For this measurement we use the basic cavity. Unfortunately the HEMT amplifier in our measurement setup is broken and for that we are limited in the signal-to-noise ration. In

the measurement we reach a lowest resolution of the photon number of about 7700. For the estimate of the photon number inside the cavity we use the following formula:

$$n_{\text{photon}} = \frac{P_{\text{in}}}{\hbar\nu_c\kappa} \quad (44)$$

where  $P_{\text{in}}$  is the input power in Watt,  $\nu_c \approx 21.468 \text{ GHz}$  the cavity resonance frequency for mode 3 and  $\kappa \approx 91 \text{ kHz}$  the cavity loss rate. Figure 20 shows the measured data. Within the error we do not observe a change of the Q factor for lower input powers. There are some papers which do investigate the change of the Q factor depending on the photon number which show a significant change of the Q factor for some materials [32],[33],[34]. The change, which they observed, would already be observable in the power range we measured. Since we do not observe a change in our measurement we do not have an indication that the Q factor should decrease for lower photon numbers. To be sure we should repeat the measurement the main experiment.

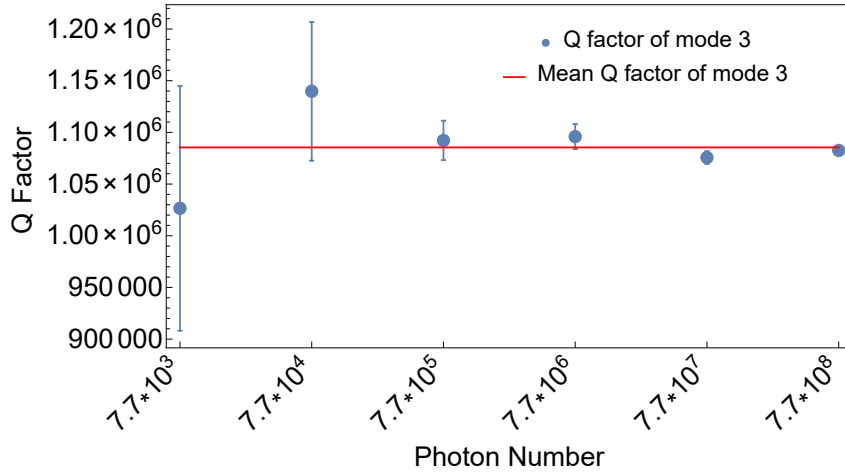


Figure 20: Measured Q factors for different input power which is related to the photo number inside the cavity. The measurement showed no in- nor decrease of the Q factor for the measured input power.

#### 4.7.2 Magnetic field

Since there are magnetic fields from other laboratories we investigate if we see a change in Q factor for different magnetic fields. This is done with the basic cavity. A coil is put around the cavity which is connected to a current source. Because of the Meissner effect we warm up the cavity above the critical temperature for each change in the magnetic field and then cool it

down again. The strength of the magnetic field changes from 0 to 38 times the earth magnetic field strength. The magnetic field of the earth varies from 0.03 mT to 0.06 mT[35]. We chose 0.06 mT as our reference value. Niobium is a superconducting material up to a critical magnetic field of 0.15 T [36] at 4 K. So we do not break the superconductivity. Further on we do not observe a significant change of the Q factor for changing magnetic fields as shown in figure 21.

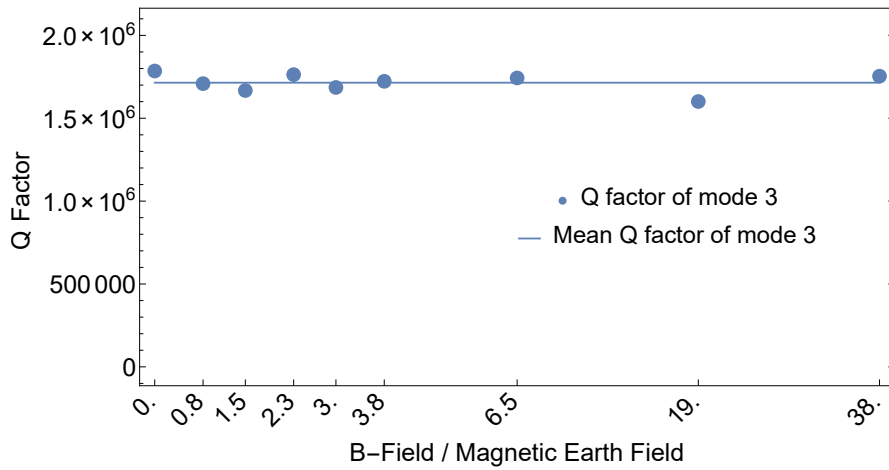


Figure 21: Measured Q factors for different applied magnetic fields. Over all there is no evidence that the magnetic field changes the Q factor in the range of the applied magnetic field strength.

## 5 Conclusion and outlook

### Conclusion

In this thesis we showed that the new designed cavity fulfills the attributes in the Q factor to do QED measurements in the strong coupling regime. We showed that the resonance frequency and the Q factor in vacuum can be well described with our simulations and analytic formulas. Also a simple model based on the BCS theory is provided to estimate and describe the Q factor for superconducting materials for lower temperatures.

The effect of the electrodes, used for quadratic AC Stark shift manipulation of the Rydberg atoms, on the Q factor was described with an analytic formula and the simulation in HFSS. The measured Q factor, associated to the electrodes, showed a quantitative good agreement with the simulation and a principal agreement with the analytic model for the third mode.

$$\begin{aligned}Q_{ele.,meas.} &= 1'293'000 \pm 113'000 \\Q_{ele.,sim.} &= 1'379'000 \\Q_{ele.,theo.} &= 1'525'000\end{aligned}$$

The total Q factor for the cavity with the electrodes is:

$$Q = 689'000 \pm 32'000$$

This shows that the Q factor is still high enough for measurement in the strong coupling regime. Further we also measured the effect of the electrodes for mode 1, 2 and 4 and saw an expected decrease.

To have interaction from the electrical field of the cavity with the Rydberg atoms two entrance holes are needed. The effect of the entrance hole width on the Q factor was simulated in HFSS and showed a significant influence for diameters larger than 2.0 mm. We measured the total Q factor for increasing entrance hole width and saw a significant effect for a diameter of 2.30 mm. For still having a high Q factor we stopped at this point. The final Q factor for a diameter of 2.30 mm of mode 3 with the electrodes is:

$$Q_{mode\ 3} = 608'000 \pm 12'000$$

### Outlook

The next step would be to mount the niobium cavity into the setup of the main experiment. There we have better possibilities to measure the temperature dependence of the Q factor and the influence of the photon number on the Q factor. Our results on the Q factor imply the possibility to



get into the strong coupling regime for a reasonable atom number of  $N=1000$ . Therefore dispersive shift measurements with this cavity are planned in the near future. An optional investigation would be to find a method to easily tune the resonance frequency of the cavity while having it in the main setup.

## **Acknowledgment**

I would like to thank Mathias Stammeier for his support during the whole time of my semester thesis. He always took time to explain and discuss all kinds of aspects of the experiment with me, gave me many interesting insights to the main experiment and made me make a lot of progress in all fields needed to do proper research. At this point I also want to thank Sébastien Garcia for listening to my presentation in advance and giving me many useful inputs for it. Of course I also want to thank all members of the Quantum Device Lab at the ETH Zürich for the nice atmosphere and the pleasant time. In special I want to thank Prof. A. Wallraff for giving me the opportunity to do my semester thesis in his lab. Finally I wish the whole group a lot of success in their research and all the best for the future.

## References

- [1] Rainer Blatt and David Wineland. Entangled states of trapped atomic ions. *Nature*, 453(7198):1008–1015, 2008.
- [2] Ronald Hanson and David D Awschalom. Coherent manipulation of single spins in semiconductors. *Nature*, 453(7198):1043–1049, 2008.
- [3] Pieter Kok, W. J. Munro, Kae Nemoto, T. C. Ralph, Jonathan P. Dowling, and G. J. Milburn. Review article: Linear optical quantum computing. pages 1–41, 2005.
- [4] M H Devoret and R J Schoelkopf. Superconducting circuits for quantum information: an outlook. *Science (New York, N.Y.)*, 339(6124):1169–74, 2013.
- [5] P Rabl, D. Demille, J M Doyle, M D Lukin, R J Schoelkopf, and P Zoller. Hybrid quantum processors: Molecular ensembles as quantum memory for solid state circuits. *Physical Review Letters*, 97(1):33003, 2006.
- [6] Anders S Sørensen, Caspar H van der Wal, Lilian I Childress, and Mikhail D Lukin. Capacitive coupling of atomic systems to mesoscopic conductors. *Physical review letters*, 92(6):063601, 2004.
- [7] J M Fink, M Göppl, M Baur, R Bianchetti, P J Leek, a Blais, and a Wallraff. Climbing the Jaynes-Cummings ladder and observing its nonlinearity in a cavity QED system. *Nature*, 454(7202):315–318, 2008.
- [8] J. M. Fink, R. Bianchetti, M. Baur, M. Göppl, L. Steffen, S. Filipp, P. J. Leek, A. Blais, and A. Wallraff. Dressed Collective Qubit States and the Tavis-Cummings Model in Circuit QED. *Physical Review Letters*, 103(8):083601, 2009.
- [9] Josephine B. Chang, Michael R. Vissers, Antonio D. Corcoles, Martin Sandberg, Jiansong Gao, David W. Abraham, Jerry M. Chow, Jay M. Gambetta, Mary Beth Rothwell, George A. Keefe, Matthias Steffen, and David P. Pappas. Improved superconducting qubit coherence using titanium nitride. *Applied Physics Letters*, 103(1):012602, 2013.
- [10] Serge Haroche and Jean-Michel Raimond. *Exploring the Quantum: Atoms, Cavities and Photons*. Number 1. 2006.
- [11] Michael Tavis and Frederick W. Cummings. Exact solution for an N-molecule-radiation-field Hamiltonian. *Physical Review*, 170(2):379–384, 1968.

- [12] Michael Tavis and Frederick W. Cummings. Approximate solutions for an N-molecule-radiation-field Hamiltonian. *Physical Review*, 188(2):692–695, 1969.
- [13] J. M. Raimond, M. Brune, and S. Haroche. Colloquium: Manipulating quantum entanglement with atoms and photons in a cavity. *Reviews of Modern Physics*, 73(3):565–582, 2001.
- [14] Alexandre Blais, Ren-Shou Huang, Andreas Wallraff, S. M. Girvin, and R. J. Schoelkopf. Cavity quantum electrodynamics for superconducting electrical circuits: An architecture for quantum computation. *Physical Review A*, 69(6):062320, 2004.
- [15] T. Thiele, S. Filipp, J. A. Agner, H. Schmutz, J. Deiglmayr, M. Stammeier, P. Allmendinger, F. Merkt, and A. Wallraff. Manipulating Rydberg atoms close to surfaces at cryogenic temperatures. *Physical Review A*, 90(1):013414, 2014.
- [16] Silvia Ruffieux. Towards cavity QED experiments with Rydberg atoms coupled to a 3D microwave cavity. (October), 2014.
- [17] D. Pozar. *Microwave Engineering Fourth Edition*. 2005.
- [18] Robert E. Collin. *Foundations for Microwave Engineering*, volume 13. 1967.
- [19] W H Hartwig and D Grissom. Dielectric Dissipation Measurement below 7.2 K. pages 1243–1247, 1965.
- [20] L I Berger and B W Roberts. Properties of superconductors. *CRC Handbook of Chemistry and Physics*, pages 12–56, 12–70, 2009.
- [21] Hasan Padamsee, Jens Knobloch, and Tom Hays. *RF superconductivity for accelerators*. 2008.
- [22] J. Bardeen, L. N. Cooper, and J. R. Schrieffer. Theory of superconductivity. *Physical Review*, 108(5):1175–1204, 1957.
- [23] J. Halbritter. MATERIAL SCIENCE OF Nb RF ACCELERATOR CAVITIES : WHERE DO WE STAND 2001 ? *Workshop on RF Superconductivity*, pages 292–301, 2001.
- [24] Hasan Padamsee. The science and technology of superconducting cavities for accelerators. *Superconductor Science and Technology*, 14(4):R28–R51, 2001.
- [25] H. Pfister. Superconducting cavities. *Cryogenics*, 16(1):17–24, 1976.

- [26] G. Schmidt and W.H. Keesom. New measurements of liquid helium temperatures. *Physica*, 4(10):971–977, 1937.
- [27] C. J. Grebenkemper Hagen and J. P. The Dielectric Constant of Liquid Helium. *Physical Review*, 80(1):89, 1950.
- [28] G.K White. Thermal expansion of vanadium, niobium, and tantalum at low temperatures. *Cryogenics*, 2(5):292–296, 1962.
- [29] R. J. Corruccini and J. J. Gniewek. *Thermal expansion of technical solids at low temperatures*. 1961.
- [30] R. Roberge. Lattice parameter of niobium between 4.2 and 300 K. *Journal of the Less Common Metals*, 40(1):161–164, 1975.
- [31] Von Hannes-Dieter Erfling. Studium zur thermischen Ausdehnung fester Stoffe in tiefer Temperatur. In *Studien zu thermischen Ausdehnung*. 1942.
- [32] R. Barends, N. Vercruyssen, A. Endo, P. J. de Visser, T. Zijlstra, T. M. Klapwijk, P. Diener, S. J. C. Yates, and J. J. A. Baselmans. Minimal resonator loss for circuit quantum electrodynamics. *Applied Physics Letters*, 97(2):023508, 2010.
- [33] Daniel L. Creedon, Yarema Reshitnyk, Warrick Farr, John M. Martinis, Timothy L. Duty, and Michael E. Tobar. High Q-factor sapphire whispering gallery mode microwave resonator at single photon energies and millikelvin temperatures. *Applied Physics Letters*, 98(22):130–133, 2011.
- [34] C. Song, M. P. DeFeo, K. Yu, and B. L. T. Plourde. Reducing microwave loss in superconducting resonators due to trapped vortices. *Applied Physics Letters*, 95(23):232501, 2009.
- [35] Carl R. (Rod) Nave. *Magnetic Field of the Earth*, 2015.
- [36] K Saito and Oho Tsukuba-shi. Critical Field Limitation of the Niobium Superconducting Rf Cavity. pages 583–587, 2001.
- [37] Jack W Ekin. APPENDIX DATA TABLES FROM EXPERIMENTAL TECHNIQUES FOR LOW-TEMPERATURE MEASUREMENTS : Cryostat Design , Material Properties , and Superconductor Critical-Current Testing National Institute of Standards and Technology Appendix Table of Contents Data Handboo. *Experimental Techniques for Low-Temperature Measurements*, 2011.

## Appendix

### A Calculation of electrode Q factor

We go through the calculation of the electrodes Q factor using the theoretical model in eq. (16) to calculate the loss from the electrodes. For  $H_t$  we use (12) with  $z = 0$  and  $x = \frac{a}{3}$  where  $a/3$  is the knot point for the first electrode. Because the cavity is symmetric we do the calculation just for one electrode and then inverse add it twice. The radius of the electrodes is 0.25 mm and they are made of copper. In the formula for the surface resistance we use the estimated conductivity of copper  $\sigma_{Cu} = 23.2 \cdot 10^7 s/m$ . By doing the integration from 0 to d, where d is the length of the electrode, we get the loss for one electrode:

$$P_{loss} = 1.01 \cdot 10^{-13} W$$

The total stored energy of the cavity by using eq. (14) is given as:

$$2 * W_e = 2.23 \cdot 10^{-18} W$$

Using eq. (17),(23) and the resonance frequency  $\nu_c \approx 21.468 GHz$  from the vacuum measurement we obtain a Q factor for one and both electrodes:

$$Q_{one\ ele.,theo.} = 2.993 \cdot 10^6$$
$$Q_{ele.,theo.} = \left( \frac{1}{Q_{one\ electrode}} + \frac{1}{Q_{one\ electrode}} \right)^{-1} = 1.497 \cdot 10^6$$

## Declaration of originality

The signed declaration of originality is a component of every semester paper, Bachelor's thesis, Master's thesis and any other degree paper undertaken during the course of studies, including the respective electronic versions.

Lecturers may also require a declaration of originality for other written papers compiled for their courses.

I hereby confirm that I am the sole author of the written work here enclosed and that I have compiled it in my own words. Parts excepted are corrections of form and content by the supervisor.

**Title of work** (in block letters):

Superconducting 3D Microwave Cavity for QED Experiments with Rydberg Atoms

**Authored by** (in block letters):

*For papers written by groups the names of all authors are required.*

**Name(s):**

Forrer

**First name(s):**

Andres

With my signature I confirm that

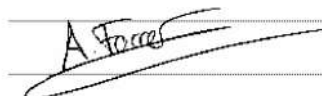
- I have committed none of the forms of plagiarism described in the 'Citation etiquette' information sheet.
- I have documented all methods, data and processes truthfully.
- I have not manipulated any data.
- I have mentioned all persons who were significant facilitators of the work.

I am aware that the work may be screened electronically for plagiarism.

**Place, date**

Zürich, 02.02.2016

**Signature(s)**



*For papers written by groups the names of all authors are required. Their signatures collectively guarantee the entire content of the written paper.*